

On the Galactic Halos Rotation by *Planck* Data

Noraiz Tahir ^{1,2,*}, Francesco De Paolis ^{1,2,3}, Asghar Qadir ⁴,
Achille A. Nucita ^{1,2,3}

¹ Department of Mathematics and Physics “Ennio De Giorgi”, University of Salento,
Via per Arnesano, I-73100 Lecce, Italy;

francesco.depaolis@le.infn.it (F.D.P.); achille.nucita@le.infn.it (A.A.N.)

² INFN, Sezione di Lecce, Via per Arnesano, I-73100 Lecce, Italy

³ INAF, Sezione di Lecce, Via per Arnesano, I-73100 Lecce, Italy

⁴ Abdul Salam School of Mathematics, G. C. University, Lahore 54600, Pakistan;
asgharqadir46@gmail.com (A.Q.)

January 10, 2023

Abstract

As galactic halos are not directly visible, there are many ambiguities regarding their composition and rotational velocity. Though most of the dark matter is non-baryonic, *some fraction is*, and it can be used to trace the halo rotation. Asymmetries in the CMB towards M31 had been seen in the Planck data and ascribed to the rotational Doppler shift of the M31 halo. Subsequently, the same methods were used in the direction of five other galaxies belonging to the Local Group, namely M33, M81, M82, NGC 5128, and NGC 4594. It had been proved that there could be stable clouds of gas and dust in thermal equilibrium with the CMB at 2.7 K, which had been called “virial clouds”. In this paper, adopting this scenerio, an attempt is made to constrain the fraction of dust grains and gas molecules in the clouds.

Keywords: cosmic microwave background; spiral galaxies; molecular clouds; dark matter; baryons

1 Introduction

According to the standard cosmological model (Λ CDM) baryons contribute $\sim 5\%$ of the Universe, of which we have only seen about half (Bertone , 2010(@); Burdzyuzha , 2020; Pérez de los Heros , 2020). Where the rest of them are and how they can be detected are still open questions. This is the so-called “missing baryon problem” (see e.g., Shull et al. (2012); Driver (2021)). It has been suggested that the missing baryons might have been ejected from the galaxies into the intergalactic medium (IGM), and a *fraction* of that component may be present in the warm-hot medium around galaxies, at temperatures of about 10^5 – 10^7 K (for details see Refs. (Cen et al. , 1999, 2006; Fraser et al. , 2011; Gupta et al. , 2012)). On the other hand, it is also suggested that a non-negligible fraction of these baryons are in the form of “cold gas clouds” spread out in the galactic halos (De Paolis et al. , 1995a; Gerhard et al. , 1996; Pifenniger et al. , 1994; Palla et al. , 1983).

In 1995, it was proposed that there may be molecular hydrogen (H_2) clouds in galactic halos at exactly the CMB temperature, so that they do not stand out against it (De Paloio et al. , 1995). It had been assumed, without suggesting any model or mechanism for it, that the clouds remain stable and avoid further gravitational collapse. It has been argued that cold clouds *could not* be in equilibrium with the CMB, as they would not be able to absorb the long wavelengths in it (Alcock et al. , 1993; De Rújula et al. , 1991), and so would have to collapse. To see such clouds merged in the CMB, in galactic halos, it was suggested that one look for γ -ray scintillation due to cosmic rays striking the H_2 molecules in the clouds. Observations by EGRET did display an excess of diffuse γ -ray emission in the halo of the Milky Way, but it could also have been due to unresolved sources in the Galaxy or from high-latitude inverse Compton scattering (see (Dixon et al. , 1998; De Paloio et al. , 1998; Kalberla et al. , 1999)). Another suggestion for detecting the claimed gas clouds is to look for an

asymmetric Doppler shift due to the rotation of the galaxies. The suggestion had been to consider our sister galaxy Andromeda (M31), and assume that the clouds rotate with the whole M31 halo. It is clear that the rotation would induce a red-shift or a blue-shift of the emitted electromagnetic signal depending on the rotation direction with respect to the observer (De Paolis et al. , 1995b).

In a series of papers, first with the analysis of WMAP and then of *Planck* data, CMB data was used to trace the halos of some nearby galaxies (De Paolis et al. , 2011, 2014; De Palois et al. , 2015; Gurzadyan et al. , 2015; De Paolis et al. , 2016; Gurzadyan et al. , 2018; De Paolis et al. , 2019) to determine whether if the data supports the Doppler shift explanation of the temperature asymmetry. The data uncovered it, not only for the galactic disks but also for some galactic halos. Further support for the Doppler shift came from the observation that the temperature asymmetry was almost frequency-independent.

In summary, there is no doubt that this phenomenon is seen in several nearby galaxies. It remains to investigate whether it is related to cold halo gas clouds, with or without dust contamination, or is due to other effects. As a working hypothesis here, we assume that it is caused, at least in part, by virial clouds populating the galactic halos. For this purpose, we model these clouds and estimate their physical parameters.

This paper aims to present a model to see the change in the physical parameters of virial clouds when they are contaminated by different percentages of dust grains. Then we will try to estimate the rotational velocity of the halos of several nearby edge-on spiral galaxies, which show a consistent temperature asymmetry in the CMB data as observed by the *Planck* satellite and already analyzed. The gas and dust clouds had been modeled previously in Refs. Tahir et al. (2019,?) by using ad-hoc boundary conditions and then the halo rotational velocities of the above-mentioned spiral galaxies estimated. We now use a more reliable model described in detail in Ref. Qadir et al. (2019) to estimate the physical parameters of virial clouds with contamination of halo dust grains in them.

The plan of the paper is as follows: in Section 2, the physical parameters of virial clouds are estimated, as a function of the fraction of molecular hydrogen (H_2), helium (He) and interstellar dust. In Section 3, the adopted models describing the distribution of the gas clouds in the halo of the considered galaxies (M31, M33, M81, M82, NGC 5128, and NGC 4594) are briefly described. These models are those generally adopted for describing the halo dark matter distribution and include the Navarro–Frenk–White (NFW), Moore, and Burkert models. Using these models, we then derive the distribution of the virial clouds and the cloud-filling factor. Then, in Section 4, we give an expression to estimate the galactic halo rotational velocity. In Section 5, the halo rotational velocity is estimated, assuming that each virial cloud is optically thick and the whole halo is composed of such clouds. However, the results obtained can be easily generalized to the case in which the virial clouds constitute only a fraction of the galactic halo dark matter and, even if less straightforwardly, to the not-optically thick clouds. Finally, in Section 6, the obtained results are discussed.

2 Virial Cloud Model

Virial clouds populating the galactic halos are assumed to be spherically symmetric and at a temperature equal to that of the CMB, i.e., $T \simeq 2.7$ K. Each cloud is assumed to be composed of molecular hydrogen, helium, and interstellar dust grains with different fractions. It has been suggested that galactic halos contain interstellar dust grain fraction of about 1–3% in mass, and the rest is H_2 , He and other heavier molecules (Imara et al. , 2018; Draine , 2003). Halo dust grains are expected to be at a slightly higher temperature with respect to that of the gas, about 5 K or so, depending on the cloud position within the galactic halo (Yershov et al. , 2020), but as a first approximation, we assume here that dust and gas are at the same temperature, i.e., 2.7 K.

There is no doubt that interstellar dust grains are found in galactic halos. It can be easily expected that dust grains form in the disk, and then the radiation pressure from disk stars, exerting a force on the dust grains, can push them towards the external regions of galaxies Ferrara et al. (1991). This force can move the dust grains to high galactic latitudes via dust-gas coupling. This process is similar to the driving agent of cool winds in giant stars (Salpeter , 1974; Kwok , 1975). Once these grains are above the disk, i.e., in the galactic halo, the the radiation pressure can expel the grains out of the galaxy environment (Chiao et al. , 1972; Greenberg et al. , 1987; Barsella et al. , 1989). The important question that needs to be answered is then to quantitatively estimate how much these dust grains contaminate the galactic halos.

Now, an objection possibly arising is whether magnetic fields and the particle destruction rate in the hot halos can play a major role in the dust grain evolution so that, eventually, these grains might not move outside the hot halo environment. In this respect, Ferrara et al. (1991) have shown that different dust grain compounds respond differently to ambient conditions. For example, graphites move faster than silicates, since graphite is much lighter than silicates grains, but both types of grains can reach values in excess of about 100 km s^{-1} ; thus, they can move further outside the halos depending upon the halo gas temperature, galaxy mass, and radiation pressure coefficients. It is also found in the literature that most of the halo dust grains are in the form of amorphous carbon, and silicates, all the other kinds of molecules and atoms that are thought to be present might be dominated by the effects of the hot gaseous halos, i.e., the high radiation pressure and magnetic field. Hence, the molecules and atoms other than graphite and silicates might not be able to reach the outer parts of the halos. So, these outer regions of the halos might contain traces of amorphous carbon and silicate dust grains, whose masses are quite similar. Therefore, the average mass of a single halo dust grain can be assumed to be $\simeq 5.65 \times 10^{-23} \text{ g}$ (Hirashita et al., 2020).

The cloud mass within the galactocentric distance r can be written as

$$M_{cl}(r) = \alpha M_{H_2}(r) + \beta M_{He}(r) + \gamma M_d(r), \quad (1)$$

where α , β , and γ are the fractions of H_2 , He, and dust, with the condition that $\alpha + \beta + \gamma = 1$. Of course, $M_{H_2}(r)$, $M_{He}(r)$, and $M_d(r)$ are the total mass of H_2 , He and dust within the distance r . If the cloud is at the CMB temperature; hence, the CMB can be considered a heat bath for the virial clouds. One can use the canonical ensemble distribution to obtain the density profile of these clouds, which can be written as

$$\rho_{cl}^3(r) = \left(\frac{512\pi^{9/2}}{3^{9/2}} \right) \left(\frac{G}{kT} \right)^{9/2} (\rho_{c_{H_2}} \rho_{c_{He}} \rho_{c_d})^{3/2} \times (m_{H_2} m_{He} m_d)^{5/2} \delta, \quad (2)$$

where

$$\delta = \exp[-(A + B + C)]. \quad (3)$$

Here,

$$A = \frac{\alpha G M_{H_2}(r) m_{H_2}}{r k T}, \quad (4)$$

$$B = \frac{\beta G M_{He}(r) m_{He}}{r k T}, \quad (5)$$

and

$$C = \frac{\gamma G M_d(r) m_d}{r k T}. \quad (6)$$

Here, G is Newton's gravitational constant, k is the Boltzmann constant, T is the cloud temperature, $\rho_{c_{H_2}}$, $\rho_{c_{He}}$, and ρ_{c_d} are the central density of H_2 , He and dust, m_{H_2} , m_{He} , and m_d are the masses of the single H_2 molecule, He atom, and halo dust grain, respectively. Taking the natural logarithm of Equation (2), and then substituting the obtained expression in Equation (1), we obtain

$$\alpha M_{H_2}(r) m_{H_2} + \beta M_{He}(r) m_{He} + \gamma M_d(r) m_d = -\frac{3rkT}{4\pi G} \ln \left(\frac{\rho_{cl}(r)}{\lambda} \right), \quad (7)$$

where $\lambda = (8\pi^{3/2}/3^{3/2})[G/(kT)]^{3/2}(\rho_{c_{H_2}}\rho_{c_{He}}\rho_{c_d})^{1/2}[m_{H_2}m_{He}m_d]^{5/6}$. The boundary conditions are at $r = 0$, where $\rho_{cl} \rightarrow \rho_c$, and $(d\rho(r)/dr)|_{r \rightarrow 0} = 0$. Taking the derivative of Equation (2) with respect to r and using Equation (7), we obtain the following differential equation

$$\begin{aligned} r \frac{d\rho_{cl}(r)}{dr} - r^2 \left(\frac{2\pi G}{kT} \right) [\rho_{cl}(r)(\alpha \rho_{c_{H_2}} m_{H_2} + \beta \rho_{c_{He}} m_{He} + \gamma \rho_{c_d} m_d)] \\ - \rho_{cl}(r) \ln \left(\frac{\rho_{cl}(r)}{\lambda} \right) = 0, \end{aligned} \quad (8)$$

In Figure 1, we give the density profile of virial clouds with different fractions of dust, i.e., $\gamma = 0.01$ (red curve), 0.02 (black curve), and 0.03 (blue curve). As one can see, by increasing the contamination of dust grains, the cloud's central density remains approximately the same, but the size of the cloud decreases, and so as its mass. This occurs because heavier molecules are pulled in more with gravity, so the cloud shrinks in size. In Table 1, we give the physical parameters (cloud central density, Jeans mass, and radius) of the three fluids virial cloud with different values of the parameters α , β , and γ .

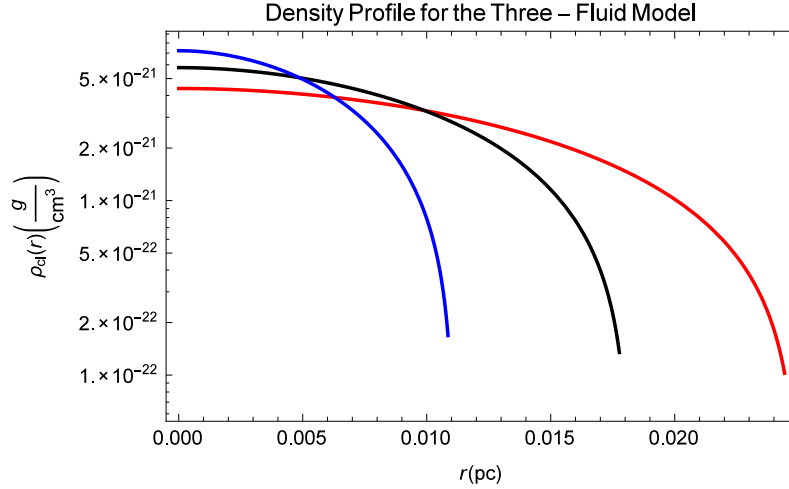


Figure 1: The density profile of three fluids virial cloud with different fractions of H_2 , He, and dust. The red curve is for parameter values $\alpha = 0.74$, $\beta = 0.25$, and $\gamma = 0.01$; the black curve corresponds to the profile for $\alpha = 0.74$, $\beta = 0.24$, and $\gamma = 0.02$; the blue curve is obtained in the case of $\alpha = 0.73$, $\beta = 0.24$, and $\gamma = 0.03$.

α	β	γ	ρ_c ($10^{-21} \text{ g cm}^{-3}$)	M_J M_\odot	R_J pc
0.74	0.01	0.25	1.44	0.020	0.025
0.74	0.02	0.24	1.79	0.019	0.018
0.73	0.03	0.24	2.04	0.017	0.011

Table 1: Physical parameters of three fluids virial cloud. The virial cloud central density, Jeans mass, and radius are given for three different choices of the parameters α , β , and γ , which define the cloud composition (see text for details).

3 Virial clouds distribution in the galactic halos

As next, we assume that a fraction f of the galactic halo dark matter is in the form of virial clouds. If these clouds are contributing to the halo dark matter, we can say that their distribution follows the dark matter distribution profile, which is generally modeled by using the Navarro–Frenk–White (NFW), the Moore, and the Burkert density profiles [Navarro et al. \(1996\)](#); [Moore et al. \(1999\)](#); [Burkert \(1995\)](#). These radial density profiles are, respectively,

$$\rho_N(r) = \frac{\rho_\circ^N}{\left(\frac{r}{r_\circ^N}\right) \left(1 + \frac{r}{r_\circ^N}\right)^2}, \quad (9)$$

(NFW model)

$$\rho_M(r) = \frac{\rho_\circ^M}{\left(\frac{r}{r_\circ^M}\right)^{1.5} \left(1 + \left(\frac{r}{r_\circ^M}\right)^{1.5}\right)}, \quad (10)$$

(Moore model)

and

$$\rho_B(r) = \frac{\rho_\circ^B}{\left(1 + \frac{r}{r_\circ^B}\right) \left(1 + \left(\frac{r}{r_\circ^B}\right)^2\right)}. \quad (11)$$

(Burkert model).

Here, $r_\circ^{N,M,B}$ are the halo core radius of the adopted models, and $\rho_\circ^{N,M,B}$ are the relative core densities. It can be easily seen that the core density corresponds to the central density of the considered galactic model. Of course, the values of both the core radius and core density depend on the considered

Galaxy	i (deg)	r_{\circ}^N kpc	r_{\circ}^M kpc	r_{\circ}^B kpc	ρ_{\circ}^N (g cm ⁻³)	ρ_{\circ}^M (g cm ⁻³)	ρ_{\circ}^B (g cm ⁻³)
M31	77	16.5	31	9.1	3.06×10^{-24}	5.05×10^{-24}	1.25×10^{-23}
M33	59	35	18	12	7.00×10^{-25}	7.60×10^{-26}	5.00×10^{-25}
M81	14	10	18	8.9	5.10×10^{-24}	7.65×10^{-25}	3.68×10^{-24}
M82	26	11	13	9	4.00×10^{-27}	1.79×10^{-27}	6.29×10^{-27}
NGC 5128	14.6	21	12	9.8	1.67×10^{-25}	4.40×10^{-25}	1.00×10^{-24}
NGC 4594	83	4.5	7.4	3.2	1.96×10^{-22}	3.18×10^{-23}	3.93×10^{-22}

Table 2: Adopted physical parameters for the NFW, Moore, and Burkert models for each considered galaxy. Note: For each considered galaxy, indicated in column 1, the inclination angle i is given in the second column, the core radius for each adopted model is also given (columns 3–5), together with the respective core density (columns 6–8).

halo model and are given in columns 3–8 of Table 2. These values are taken from Tamm et al. (2012); Tahir et al. (2019) and are reproduced in Table 2 for the advantage of the reader.

The surface density of the virial clouds obtained in a galactic halo is given by (Lokas et al. , 2001)

$$\Sigma(a) = 2 \int_a^{\infty} \frac{r \rho_{N,M,B}(r)}{(r^2 - a^2)^{1/2}} dr. \quad (12)$$

and, therefore, the total number of virial clouds per unit area can be estimated as

$$N(a) = f \left(\frac{\Sigma(a)}{M_J} \right), \quad (13)$$

where f is the fraction of halo dark matter present in the form of virial clouds, M_J is the Jeans mass of a single virial cloud, and a is a given value of the halo projected radius.

Once we have estimated the total number of virial clouds in the three considered galactic dark matter halo models using Equation (13), we are in the position to estimate the cloud filling factor S , which is actually the ratio of the area covered by all the clouds within the halo radius R and the total projected area and is given by

$$S(\leq R) = \frac{\int_0^R 2\pi a N(a) r_{cl}^2 da}{\int_0^R 2\pi a da}, \quad (14)$$

where r_{cl} is the virial cloud radius, and M_{cl} its mass.

4 Estimating the galaxy halo rotational velocity

Starting from the cumulative radial distribution of the virial clouds and considering the temperature asymmetry in the CMB data towards a given galaxy, we can then estimate the halo rotational velocity, which is given by

$$v_{\text{rot}} = \left(\frac{\Delta T}{T} \right) \left(\frac{c}{2 \sin(i) S f \langle \tau \rangle} \right), \quad (15)$$

where c is the light speed in a vacuum, i is the inclination angle of the considered galaxy, S is the virial cloud filling factor as calculated from Equation (14), $\langle \tau \rangle$ is the average optical depth of the virial clouds, and $\Delta T/T$ is the temperature asymmetry detected in the CMB towards the two opposite quadrants of the galactic halo (for details see (De Paolis et al. , 2014; De Paolis et al. , 2015; Gurzadyan et al. , 2015; De Paolis et al. , 2016; Gurzadyan et al. , 2018; De Paolis et al. , 2019)). The values of $\Delta T/T$ are obtained from the *Planck* data analyzed for the SMICA band and previously analyzed in Refs. De Paolis et al. (2016); Gurzadyan et al. (2018); Tahir et al. (2019). For estimating v_{rot} , we assume, as a first approximation, that the virial clouds are characterized by $\langle \tau \rangle \simeq 1$, which means that the virial clouds are assumed to emit as black bodies at the CMB temperature. However, one needs to estimate the average optical depth of the virial clouds, $\langle \tau \rangle$, over a detector frequency range, $\nu_1 - \nu_2$, which is, therefore, given as $\langle \tau \rangle = \frac{1}{\nu_1 - \nu_2} \int_{\nu_1}^{\nu_2} \tau_{\nu} d\nu$. The evaluation of

this relation allows for determining whether the considered virial clouds are optically thick or thin. An alternative way to check the stability of the virial clouds is by estimating the “stability time” of these clouds, which is related to the probability of interaction of the molecules contaminating the virial clouds with the CMB photons. In [Qadir et al. \(2019\)](#), it was estimated the stability time for the virial clouds composed of purely H_2 molecules. The estimated stability time results are much less than the collapsing time of the cloud, which showed that these clouds become stable before they could collapse. The considered situation was very simple, but when dust and heavier molecules are assumed to contaminate the clouds, the stability time and the collapsing time could vary because there could be quantum effects coming in, i.e., additional translational, rotational, and vibrational modes due to the interaction of the incoming radiation with heavier and complex molecules.

5 Halo Model

The aim of this section is to implement the generalized model we give in the previous sections, to the considered galaxy halos. As a first approximation, we assume that all the dark matter in the considered galactic halos is in the form of virial clouds. We also assume, for definiteness, that a dust grain mass fraction contamination of the order of 1–3% is present in the considered galaxy halos.

We start by modeling the M31 galactic halo, and then we extend our analysis considering the other galaxies. Following [Tamm et al. \(2012\)](#), we assume that the M31 halo size is $R \simeq 200$ kpc. However, the reader should keep in mind that there is not a definite estimate for the size of the M31 halo. For example, [Lehner et al. \(2020\)](#) used ultraviolet absorption measurements of Si II, Si III, Si IV, C II, and C IV from the Hubble Space Telescope/Cosmic Origins Spectrograph and O IV from the far Ultraviolet Spectrographic Explorer to estimate how metals are distributed in the circumgalactic medium (CGM) of M31 and found that the halo of M31 might extend up to ≈ 300 kpc.

In [Figure 2](#), we give the cloud filling factor obtained through [Equation \(14\)](#). It is seen that for all the considered virial cloud models, the filling factor turns out to be less than 1. It is also seen that the obtained values of the filling factor for the three dark matter models when we consider three fluids virial clouds are more or less the same.

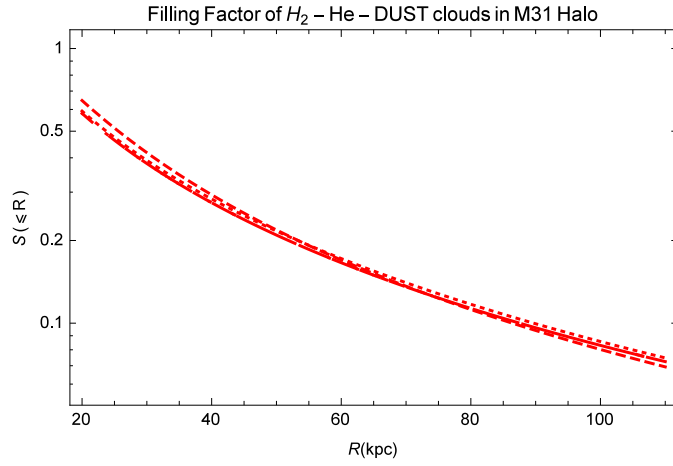
The virial cloud cumulative radial distribution towards the M31 halo, for a dust concentration fraction in the range 1–3%, is shown in [Figure 3](#), assuming $f = 1$. From these plots, it is clear that the number of virial clouds in the M31 halo does not depend strongly on the considered halo model, but it depends more heavily on the cloud chemical composition and dust abundance.

We are now in a position to estimate the rotational velocity of the M31 halo, within various galactocentric distances using [Equation \(15\)](#). We use the SMICA processed data to obtain the values of ΔT for M31 galaxy, which is already analyzed in ([Tahir et al. , 2019](#)). The SMICA data were chosen because they are less contaminated than the other available *Planck* bands. We estimated the rotational velocity values within 41.5 kpc to 103.8 kpc, and the obtained results are shown in [Table 3](#).

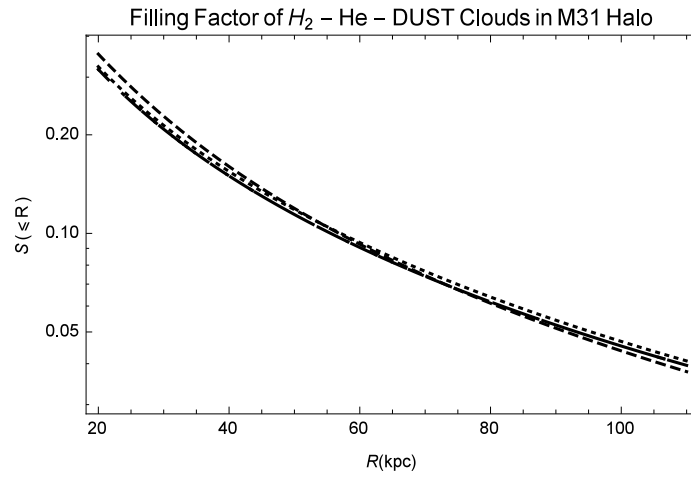
We remark here that HI observations towards the Andromeda galaxy obtained with the Effelsberg and Green Bank 100 m telescopes showed that the rotation curve in the M31 disk up to a galactocentric distance ≈ 35 kpc, is approximately flat with velocity ≈ 226 km/s. Moreover, M31 rotation curves up to a galactocentric distance ≈ 100 kpc were built by combining disk rotation velocities and radial velocities of satellite galaxies and globular clusters. Ref. [Carigana et al. \(2006\)](#) adopted the NFW model to estimate these curves obtaining an approximately flat behavior with $v_{rot} \approx 110$ –200 km/s. However, as already noted, the M31 halo rotation velocity is much less constrained by observations with respect to the disk rotational velocity. In particular, from [Table 3](#), we see that for $f = 1$, the rotational velocity of the M31 halo follows a trend similar to that obtained for the disk, for the virial cloud model with 1% , 2%, and 3% contamination of dust grains. The estimated M31 halo rotational velocity turns out to be $v_{rot} \approx 50$ –230 km/s, at large galactocentric distances (that is, in the region between about 20 kpc and 108 kpc from the M31 center).

Similarly, in the case of other spiral galaxies, we can apply the same procedure like M31 for estimating the halo rotational velocity of the other considered galaxies, namely M33, M81, M82, NGC 5128, and NGC 4594, respectively. We also assumed that 1–3% of dust contaminate virial clouds present in the halos of these galaxies, and $f = 1$ is used as a reference value in [Tables 3–8](#).

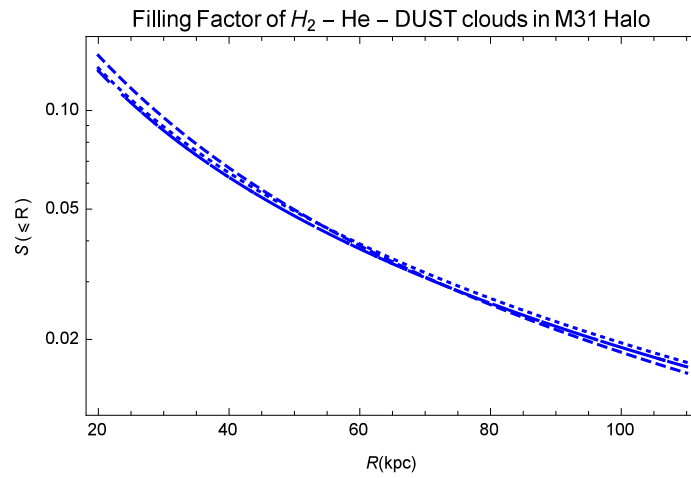
The total number of virial clouds per unit area, the filling factor of the clouds in each considered galaxy halo, and the halo rotational velocity are shown in [Tables 3–8](#). We have used the temperature asymmetry data published in the literature (see in particular the [De Paolis et al. \(2014\)](#);



(a)

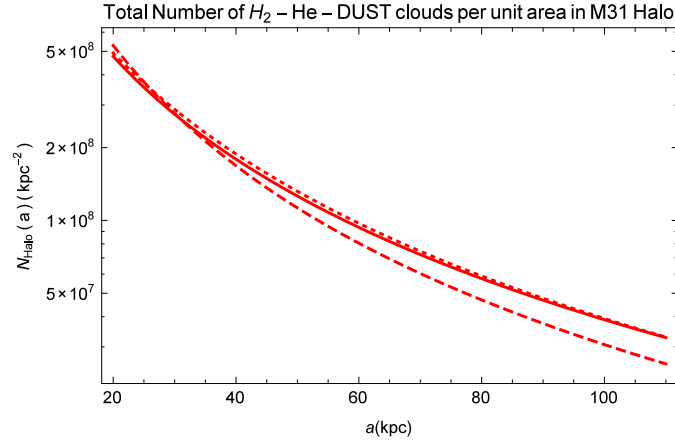


(b)

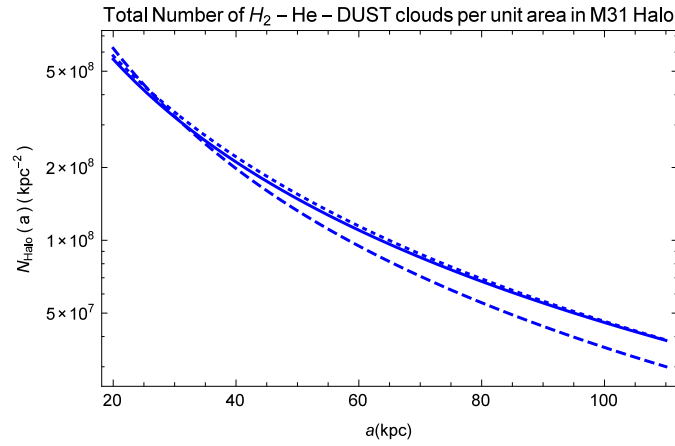


(c)

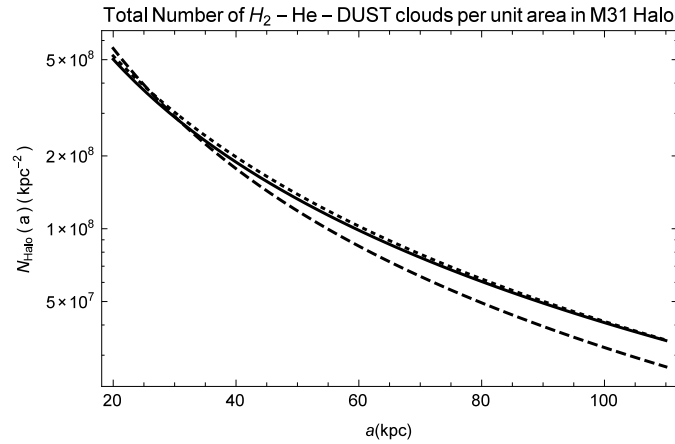
Figure 2: The filling factor for the three fluids virial cloud model with 1% (a), 2% (b), and 3% (c) dust contamination is given in the case of the M31 halo. The bold, dotted, and dashed curves correspond to the NFW, Moore, and Burkert models, respectively.



(a)



(b)



(c)

Figure 3: The cumulative radial distribution of the number of clouds per unit area for the three fluids virial cloud models with 1% (a), 2% (b), and 3% (c) dust contamination is given in the case of the M31 halo. The bold curve is for the NFW model, the dotted curve corresponds to the Moore model, while the dashed one is for the Burkert model.

f_{dust}	R (kpc)	$\Delta T/T$ (10^{-6})	N^N	N $10^8(\text{kpc}^{-2})$		N^B	S_N	S (10^{-2})			v_{rot} (km/s)	
				N^M				S_M	S_B	v_{rot}^N	v_{rot}^M	v_{rot}^B
1%	21.4	-0.98	4.36	4.52	16.25	27.20	28.28	100	-0.55	-0.53	-0.99	
	31.1	2.36	2.60	2.73	5.67	16.38	17.10	35.4	2.23	2.12	3.27	
	41.8	6.40	1.69	1.77	7.90	10.57	11.11	49.41	9.41	8.96	12.28	
	51.8	14.3	1.18	1.24	6.16	7.42	7.75	38.50	29.86	28.57	28.27	
	77.8	7.90	0.67	0.61	3.93	3.76	3.86	24.59	32.55	31.71	34.09	
	103.8	7.80	0.36	0.36	2.87	2.22	2.29	17.95	53.34	52.87	37.28	
2%	21.4	-0.98	4.59	4.76	17.11	14.89	15.43	55.45	-1.01	-0.98	-1.82	
	31.1	2.36	2.74	2.88	5.97	8.99	9.33	19.34	4.08	3.89	6.00	
	41.8	6.40	1.78	1.87	8.32	5.77	6.05	26.96	17.25	16.43	22.59	
	51.8	14.3	1.24	1.30	6.48	4.04	4.23	21.01	54.72	52.35	51.82	
	77.8	7.90	0.63	0.65	4.14	2.20	2.11	13.42	59.65	58.12	62.48	
	103.8	7.80	0.38	0.31	3.02	1.24	1.25	9.79	97.76	96.90	68.32	
3%	21.4	-0.98	5.13	5.32	19.12	6.21	6.44	23.14	-2.43	-2.35	-4.36	
	31.1	2.36	3.06	3.21	6.67	3.71	3.89	8.08	9.79	9.33	14.39	
	41.8	6.40	1.99	2.90	9.30	2.40	2.52	11.25	41.34	39.37	53.92	
	51.8	14.3	1.39	1.45	7.24	1.69	1.76	8.77	131.10	125.42	119.69	
	77.8	7.90	0.70	0.72	4.62	0.88	0.82	5.60	142.93	139.24	124.15	
	103.8	7.80	0.42	0.43	3.37	0.65	0.52	4.08	234.22	232.66	163.69	

Table 3: Estimated physical parameters of the M31 halo, populated by virial clouds with 1%, 2%, and 3% dust contamination. Note: The temperature asymmetry divided by the CMB temperature (column 3), the total number of virial clouds per unit area within the observed radius (columns 4–6), the filling factor (columns 7–9) and the estimated rotational velocity of the M31 halo (columns 10–12) are given, with respect to the considered halo radii (column 2), for the three considered dark matter models.

De Palois et al. (2015); Gurzadyan et al. (2015); De Paolis et al. (2016); Gurzadyan et al. (2018); De Paolis et al. (2019)) in the 70, 100, and 143 GHz bands in the case of M33, M81, M82, and NGC 5128, and SMICA band for NGC 5494 at a resolution corresponding to $N_{side} = 2048$, in HEALPix scheme Gorski et al. (2005). The temperature excesses are shown in Tables 4 and 5 (see column 3 for NGC 5494 and column 4 for M33, M81, M82, and NGC 5128, respectively). Tables 3–8 report the obtained values of the halo rotational velocity v_{rot} for the various adopted models and for f_{dust} ranging from 1% to 3%. As one can see, the obtained v_{rot} values are in substantial agreement with the expectations. However, in the case of some galaxies, there are regions in which apparently inconsistent values of v_{rot} are present. Considering in detail each analyzed galaxy, in the case of the M31 halo (see Table 3), the rotational velocity is acceptable for all three adopted models and for all dust fractions. In the case of NGC 5494, M33, and M81 halo, respectively (see Tables 4–6), the v_{rot} values appear acceptable for f_{dust} of 1% and 2% and only marginally acceptable for $f_{dust} = 3\%$, as a result, we believe that it is not likely to say that $f_{dust} < 3\%$ for these galaxies. In the case of the M82 halo (see Table 7) at a large radius for all the dust concentrations, the v_{rot} values are not acceptable hence we can say that at larger radius $f_{dust} < 1\%$. In the case of NGC 5128 halo (see Table 8), the rotational velocity values appear acceptable for all the cases.

Notice that the obtained v_{rot} values depend on the following assumptions: (1) We assume a constant dust fraction in each galaxy, independent of the galactocentric distance. However, as is explained previously that the dust grain temperature can easily be higher. It should be borne in mind that dust grains in the halo follow a distribution profile that depends upon the galactocentric distance, and to treat this model more physically, one needs to see how these dust grains are distributed in the halos; (2) the temperature of the halo dust grains is assumed to be exactly 2.7 K (see Yershov et al. (2020)), and hence one needs to see how the temperature profile of dust changes with the galactocentric distance; (3) the distribution profile of the clouds in the halos of each considered galaxy: it can be seen that the NFW model gives more consistent results than the other two models, and (5) our assumption that the observed asymmetry in the CMB, i.e., the values of $\Delta T/T$ are solely due to virial clouds in the halo of each galaxy. However, there are other effects from a theoretical point of view that give can

f_{dust}	R (kpc)	$\Delta T/T$ (10^{-6})	N $10^8(\text{kpc}^{-2})$				S (10^{-2})			v_{rot} (km/s)		
			N^N	N^M	N^B	S_N	S_M	S_B	v_{rot}^N	v_{rot}^M	v_{rot}^B	
1%	33.4	-8.44	20.26	15.73	12.43	12.66	19.86	17.74	-10.37	-12.92	-17.25	
	66.8	-6.60	5.58	4.13	6.21	3.49	2.58	4.43	-28.53	-38.65	-42.44	
	100.2	0.36	2.56	1.85	4.87	1.60	1.16	3.13	34.54	47.75	49.14	
	167	3.66	0.95	0.67	0.57	0.59	0.42	0.18	39.32	33.67	49.58	
2%	33.4	-8.44	21.32	16.62	13.82	6.91	5.93	4.83	-18.45	-23.68	-23.71	
	66.8	-6.60	5.88	4.34	6.97	1.90	1.40	1.22	-52.33	-70.84	-60.91	
	100.2	0.36	2.70	1.95	5.13	0.87	0.63	0.64	63.30	87.51	92.91	
	167	3.66	1.00	0.70	0.30	0.32	0.22	0.09	71.00	84.25	88.93	
3%	33.4	-8.44	23.83	18.57	14.62	2.88	2.22	1.72	-44.21	-56.74	-31.42	
	66.8	-6.60	6.57	4.86	7.79	0.79	0.58	0.92	-125.50	-169.72	-143.44	
	100.2	0.36	3.02	2.18	5.74	0.36	0.26	0.68	151.65	200.96	160.91	
	167	3.66	1.11	0.79	0.32	0.13	0.09	0.04	140.74	158.01	164.51	

Table 4: Same as Table 3, but for NGC 5494 halo. Note: All columns have the same meaning as Table 3, but for NGC 5494 halo.

give rise to this asymmetry in the CMB. To treat the problem of the halo rotation more physically, one has to see how the halo dust is distributed and the chemical composition of the virial clouds, for each of the above galaxies separately, and consider other possible contributing effects.

ν (GHz)	f_{dust}	R (kpc)	$\Delta T/T$ (10^{-6})	N^N	N $10^8 (\text{kpc}^{-2})$ N^M	N^B	S_N	S (10^{-2}) S_M	S_B	v_{rot}^N	v_{rot}^M (km/s)	v_{rot}^B
70	1%	92	25.68	3.13	7.26	1.35	19.20	4.50	8.46	22.92	98.95	53.17
		171	11.0	1.12	2.18	5.28	7.02	1.74	3.34	27.36	141.36	31.49
		245	5.13	0.59	1.07	3.60	3.57	6.71	2.21	24.12	134.08	21.10
	2%	92	25.68	3.30	7.65	1.42	17.89	2.43	4.65	42.04	181.33	97.45
		171	11.0	1.18	2.29	5.55	3.99	11.33	8.14	50.14	259.06	57.81
		245	5.13	6.27	1.12	3.79	20.77	3.05	1.96	44.20	245.71	38.67
	3%	92	21.4	3.69	8.55	1.59	4.21	0.13	0.19	100.63	434.35	233.47
		171	11.0	1.32	2.56	6.21	1.71	0.38	0.075	120.14	620.68	138.51
		245	5.13	7.01	1.26	4.27	0.89	0.015	0.0052	105.91	588.67	92.64
100	1%	92	22.01	3.13	7.26	1.35	19.20	4.50	8.46	19.64	84.81	45.58
		171	15.41	1.12	2.18	5.28	7.02	1.74	3.34	38.30	197.91	44.16
		245	6.60	0.59	1.07	3.60	3.57	6.71	2.21	31.01	172.38	27.13
	2%	92	22.01	3.30	7.65	1.42	17.89	2.43	4.65	36.01	135.42	83.52
		171	15.41	1.18	2.29	5.55	3.99	11.33	8.14	70.20	362.69	80.94
		245	6.60	6.27	1.12	3.79	20.77	3.05	1.96	56.83	315.91	49.71
	3%	92	22.01	3.69	8.55	1.59	4.21	0.13	0.19	86.25	372.37	200.17
		171	15.41	1.32	2.56	6.21	1.71	0.38	0.075	168.19	868.95	193.92
		245	6.60	7.01	1.26	4.27	0.89	0.015	0.0052	136.17	756.87	119.11
143	1%	92	21.46	3.13	7.26	1.35	19.20	4.50	8.46	19.15	82.69	44.44
		171	16.87	1.12	2.18	5.28	7.02	1.74	3.34	41.95	216.76	48.37
		245	7.15	0.59	1.07	3.60	3.57	6.71	2.21	33.60	186.75	29.39
	2%	92	21.46	3.30	7.65	1.42	17.89	2.43	4.65	35.10	151.54	81.44
		171	16.87	1.18	2.29	5.55	3.99	11.33	8.14	76.89	397.23	88.65
		245	7.15	6.27	1.12	3.79	20.77	3.05	1.96	61.57	342.23	53.86
	3%	92	21.46	3.69	8.55	1.59	4.21	0.13	0.19	84.10	363.06	195.11
		171	16.87	1.32	2.56	6.21	1.71	0.38	0.075	184.21	951.71	212.39
		245	7.15	7.01	1.26	4.27	0.89	0.015	0.0052	147.52	819.94	129.04

Table 5: Estimated physical parameters of the clouds in the M33 halo and its rotational velocity. Note: We give, for the considered Planck frequency band (column 1), and for each considered halo radii (column 3), the temperature asymmetry divided by the CMB temperature (column 4), the total number of virial clouds per unit area within the observed radius (column 5–7), the filling factor (column 8–10) and the estimated rotational velocity of the M31 halo (column 11–13), for the three considered dark matter models.

ν (GHz)	f_{dust}	R (kpc)	$\Delta T/T$ (10^{-6})	N $10^8(\text{kpc}^{-2})$			S (10^{-2})			v_{rot}^N	v_{rot} (km/s)	
				N^N	N^M	N^B	S_N	S_M	S_B		v_{rot}^M	v_{rot}^B
70	1%	15	20.36	14.80	15.56	18.85	0.92	0.97	0.98	13.12	12.90	48.44
		30	23.85	5.28	5.49	13.39	0.33	0.34	0.87	44.51	43.08	106.45
		60	29.35	1.63	1.62	4.60	0.10	0.10	0.28	17.84	17.91	25.8
	2%	15	20.36	15.60	16.37	13.37	0.50	0.53	0.98	24.44	23.79	88.76
		30	23.85	5.56	5.78	14.47	0.18	0.18	0.47	82.09	78.94	195.08
		60	29.35	1.71	1.71	4.84	0.055	0.055	0.15	32.69	32.83	47.30
	3%	15	20.36	17.40	18.30	13.39	0.21	0.22	0.41	54.60	57.01	212.67
		30	23.85	6.21	6.46	16.64	0.072	0.078	0.019	194.64	189.14	467.38
		60	29.35	1.92	1.91	5.41	0.023	0.023	0.063	78.33	78.67	113.97
100	1%	15	14.67	14.80	15.56	18.85	0.92	0.97	0.98	19.81	19.31	34.91
		30	20.18	5.28	5.49	13.39	0.33	0.34	0.87	37.86	36.45	90.07
		60	27.52	1.63	1.62	4.60	0.10	0.10	0.28	36.26	36.79	24.23
	2%	15	14.67	15.60	16.37	13.37	0.50	0.53	0.98	17.97	17.15	63.97
		30	20.18	5.56	5.78	14.47	0.18	0.18	0.47	69.39	66.80	165.06
		60	27.52	1.71	1.71	4.84	0.055	0.055	0.15	30.52	30.78	44.11
	3%	15	14.67	17.40	18.30	13.39	0.21	0.22	0.41	43.07	41.08	153.28
		30	20.18	6.21	6.46	16.64	0.072	0.078	0.019	166.25	160.04	395.47
		60	27.52	1.92	1.91	5.41	0.023	0.023	0.063	73.43	73.75	106.40
143	1%	15	16.51	14.80	15.56	18.85	0.92	0.97	0.98	11.03	10.52	39.27
		30	18.34	5.28	5.49	13.39	0.33	0.34	0.87	34.42	33.13	81.88
		60	27.52	1.63	1.62	4.60	0.10	0.10	0.28	16.72	16.79	24.23
	2%	15	16.51	15.60	16.37	13.37	0.50	0.53	0.98	20.22	19.29	71.97
		30	18.34	5.56	5.78	14.47	0.18	0.18	0.47	63.08	60.72	150.06
		60	27.52	1.71	1.71	4.84	0.055	0.055	0.15	30.65	30.78	44.41
	3%	15	16.51	17.40	18.30	13.39	0.21	0.22	0.41	48.45	46.22	172.44
		30	18.34	6.21	6.46	16.64	0.072	0.078	0.019	151.13	145.49	359.54
		60	27.52	1.92	1.91	5.41	0.023	0.023	0.063	73.43	73.75	106.40

Table 6: Same as Table 5 but for M81 halo. Note: All columns have the same meaning as Table 5 but for M81 galaxy halo.

ν (GHz)	f_{dust}	R (kpc)	$\Delta T/T$ (10^{-6})	N $10^8(\text{kpc}^{-2})$		N^B	S_N	S (10^{-2})		S_B	v_{rot}^N	v_{rot} (km/s)	
				N^N	N^M			S_M	S_B			v_{rot}^M	v_{rot}^B
70	1%	15	18.16	14.57	16.61	16.74	9.10	10.03	10.46	68.25	59.85	118.15	
		30	15.59	5.31	5.35	13.02	3.32	3.34	8.13	160.69	159.58	213.09	
		60	-5.87	1.66	1.49	8.03	1.04	0.93	5.04	-192.72	-214.66	-163.03	
	2%	15	18.16	15.33	17.49	17.63	4.96	5.66	5.71	125.07	109.68	216.53	
		30	15.59	5.59	5.63	13.70	1.82	1.82	4.44	294.49	294.47	390.51	
		60	-5.87	1.75	1.57	8.46	0.56	0.51	2.74	-353.18	-393.38	-298.78	
	3%	15	18.16	17.14	19.54	19.70	2.07	2.36	2.38	299.66	262.78	518.76	
		30	15.59	6.25	6.29	15.32	0.76	0.76	1.85	705.54	700.65	935.60	
		60	-5.87	1.96	1.76	9.45	0.23	0.21	1.14	-846.17	-942.46	-715.82	
100	1%	15	16.88	14.57	16.61	16.74	9.10	10.03	10.46	55.62	109.80	109.80	
		30	17.61	5.31	5.35	13.02	3.32	3.34	8.13	181.49	180.23	240.67	
		60	-6.60	1.66	1.49	8.03	1.04	0.93	5.04	-216.87	-241.49	-183.34	
	2%	15	16.88	15.33	17.49	17.63	4.96	5.66	5.71	116.23	101.92	201.22	
		30	17.61	5.59	5.63	13.70	1.82	1.82	4.44	332.60	330.29	441.05	
		60	-6.60	1.75	1.57	8.46	0.56	0.51	2.74	-397.35	-442.52	-336.12	
	3%	15	16.88	17.14	19.54	19.70	2.07	2.36	2.38	278.47	244.20	482.20	
		30	17.61	6.25	6.29	15.32	0.76	0.76	1.85	796.85	791.32	566.68	
		60	-6.60	1.96	1.76	9.45	0.23	0.21	1.14	-951.94	-900.60	-805.30	
143	1%	15	22.01	14.57	16.61	16.74	9.10	10.03	10.46	82.73	72.54	143.22	
		30	22.01	5.31	5.35	13.02	3.32	3.34	8.13	226.86	225.29	300.84	
		60	-4.40	1.66	1.49	8.03	1.04	0.93	5.04	-144.54	-160.99	-122.28	
	2%	15	22.01	15.33	17.49	17.63	4.96	5.66	5.71	151.60	132.95	262.46	
		30	22.01	5.59	5.63	13.70	1.82	1.82	4.44	415.75	412.86	551.31	
		60	-4.40	1.75	1.57	8.46	0.56	0.51	2.74	-264.89	-295.03	-224.08	
	3%	15	22.01	17.14	19.54	19.70	2.07	2.36	2.38	363.22	318.52	268.81	
		30	22.01	6.25	6.29	15.32	0.76	0.76	1.85	996.06	989.15	932.08	
		60	-4.40	1.96	1.76	9.45	0.23	0.21	1.14	-634.63	-706.85	-736.68	

Table 7: Same as Table 5 but for the case of M82 halo. Note: All columns have the same meaning as Table 5 but for M82 galaxy halo.

ν (GHz)	f_{dust}	R (kpc)	$\Delta T/T$ (10^{-6})	N^N	$\frac{N}{N^M}$ $10^8(\text{kpc}^{-2})$	N^B	S_N	$\frac{S}{S_M}$ (10^{-2})	S_B	v_{rot}^N	$\frac{v_{rot}}{v_{rot}^M}$ (km/s)	v_{rot}^B
70	1%	92	25.68	18.68	12.75	13.48	11.16	7.97	8.42	13.09	19.16	11.22
		171	11.74	6.22	3.76	6.02	3.89	2.35	3.76	17.94	29.67	38.63
		245	4.40	3.19	1.84	4.74	1.99	1.15	2.96	13.14	22.72	46.30
	2%	92	25.68	19.66	13.43	14.19	6.37	4.35	4.59	23.99	35.13	18.57
		171	11.74	6.55	3.96	6.33	2.12	1.28	2.05	32.89	54.38	57.84
		245	4.40	3.36	1.94	4.99	1.09	0.62	1.62	24.01	41.63	84.85
	3%	92	25.68	21.97	15.01	15.86	2.67	1.83	1.91	57.48	84.16	44.49
		171	11.74	7.32	4.43	7.08	0.88	0.53	0.85	78.80	130.30	78.81
		245	4.40	3.76	2.17	5.58	0.45	0.26	0.67	57.53	99.75	120.33
100	1%	92	22.01	18.68	12.75	13.48	11.16	7.97	8.42	11.22	16.43	18.68
		171	15.41	6.22	3.76	6.02	3.89	2.35	3.76	23.55	38.95	30.46
		245	6.60	3.19	1.84	4.74	1.99	1.15	2.96	19.65	34.08	69.45
	2%	92	22.01	19.66	13.43	14.19	6.37	4.35	4.59	20.56	30.11	15.94
		171	15.41	6.55	3.96	6.33	2.12	1.28	2.05	71.38	120.71	47.28
		245	6.60	3.36	1.94	4.99	1.09	0.62	1.62	62.45	127.85	139.02
	3%	92	22.01	21.97	15.01	15.86	2.67	1.83	1.91	72.14	68.13	77.63
		171	15.41	7.32	4.43	7.08	0.88	0.53	0.85	171.02	149.63	113.27
		245	6.60	3.76	2.17	5.58	0.45	0.26	0.67	130.49	93.49	97.36
143	1%	92	21.28	18.68	12.75	13.48	11.16	7.97	8.42	10.84	15.83	18.39
		171	16.88	6.22	3.76	6.02	3.89	2.35	3.76	35.80	42.66	23.83
		245	7.15	3.19	1.84	4.74	1.99	1.15	2.96	31.29	36.92	75.24
	2%	92	21.28	19.66	13.43	14.19	6.37	4.35	4.59	19.81	29.17	15.83
		171	16.88	6.55	3.96	6.33	2.12	1.28	2.05	47.28	78.18	122.38
		245	7.15	3.36	1.94	4.99	1.09	0.62	1.62	139.02	67.66	137.89
	3%	92	21.28	21.97	15.01	15.86	2.67	1.83	1.91	47.63	69.73	36.86
		171	16.88	7.32	4.43	7.08	0.88	0.53	0.85	113.27	187.31	154.35
		245	7.15	3.76	2.17	5.58	0.45	0.26	0.67	93.49	162.10	130.64

Table 8: Same as Table 5 but for NGC 5128 halo. Note: All columns have the same meaning as Table 5 but for NGC 5128 galaxy halo.

6 Results and Discussions

The observed Doppler shift [De Paolis et al. \(2011, 2014\)](#); [De Palois et al. \(2015\)](#); [Gurzadyan et al. \(2015\)](#); [De Paolis et al. \(2016\)](#); [Gurzadyan et al. \(2018\)](#); [De Paolis et al. \(2019\)](#) had been predicted earlier to search for cold gas clouds in Ref. [De Paolis et al. \(1995b\)](#), which could contain some of the missing baryons. It has since been used to try to investigate the halo rotation (see Refs. [Tahir et al. \(2019,?\)](#)). Here, the virial model in Ref. [Qadir et al. \(2019\)](#) is used to obtain more reliable and precise answers regarding the halo rotation and the composition and distribution of the clouds in the halos. For this purpose, we used the following assumptions as a first approximation: (1) all the considered halos contain 1–3% f_{dust} which remains constant throughout the halo; (2) the entire temperature asymmetry in the CMB $\Delta T/T$ we observed towards the galaxies is due to virial clouds in the halos; (3) the temperature of halo dust grains is also exactly 2.7 K; and (4) the virial clouds follow the same dark matter profile NFW, Moore or Burkert models are widely used to map the distribution of dark matter in the galactic halos.

The radial distribution of virial clouds within the M31 halo, taking $f = 1$ for definiteness, and the cumulative radial profiles were obtained by estimating the virial cloud surface density $\Sigma(a)$, by using Equation (12), and then dividing it by the mass of a single cloud (see Figure 3). It was seen that the total number of clouds per unit area for each model at large galactocentric distances was approximately the same. We then estimated the cloud-filling factor by using Equation (14). Our end goal was to estimate the rotational velocities and the viable chemical composition of the virial clouds of the galaxy halos under consideration for each of the three dark matter models, which are given in Tables 3–8. In most cases, the obtained values of the rotational velocity appear consistent with the expectations, but there appeared some inconsistent values in the estimated rotational velocity of the considered halos, which can merely be due to the values chosen for the model parameters, in particular, f_{dust} and dust temperature at 2.7 K. For example, at first, we need to see how dust grains are distributed in the halos of these galaxies and how the halo dust temperature profile can be seen in the halos. The other point concerns the assumption that the entire temperature asymmetry in the CMB is due to virial clouds. However, four other possibilities may be considered to explain the detected temperature towards the considered galactic halo: (i) the Sunyaev–Zeldovich (SZ) effect, which is the distortion of the CMB through inverse Compton scattering by high energy electrons in galaxy clusters, in which the low energy CMB photons receive an average energy boost during a collision with the high energy cluster electrons, in particular, the kinetic energy ([Matilla et al. , 2020](#)); (ii) synchrotron emission by fast-moving electrons which is a type of non-thermal radiation generated by charged particles spiraling around magnetic field lines. Since these electrons are subject to acceleration due to the change of their direction, they emit photons ([Dolag et al. , 2000](#)); (iii) free-free emission (or bremsstrahlung emission) by free electrons passing close to atomic nuclei ([Sun et al. , 2010](#)); and (iv) the anomalous microwave emission (AME) from dust grains, which is the electric dipole radiation from small spinning dust grains. The anomalous component at 53 GHz is 2.5 times as bright as the free-free emission traced by $H\alpha$, providing an approximate normalization for models with significant spinning dust emission ([Leitch , 2013](#)). The spinning dust model is thought to be the simplest explanation for the observed dust correlations, in the microwave data, but the combination of increasingly sophisticated models and observations with better frequency resolution will ultimately decide whether spinning dust can explain the detected anomalous emission. So, to analyze the rotational dynamics of galactic halos in more detail by using *Planck* data, it would be necessary to constrain the contribution of each of the effects (i)–(iv) above in the temperature asymmetry towards considered halos. In particular, the contribution of the rotational kinetic Sunyaev–Zeldovich (rkSZ) has been considered in the case of the M31 halo, and it was found that at the present level of accuracy, it gives a negligible contribution to the observed asymmetry towards M31 as seen by the *Planck* data [Tahir et al. \(2022\)](#). Consideration of the contribution of the other effects and the halo dust profile will be attempted in a separate paper.

We stress that we do not claim that the virial clouds should contain *all* the baryonic dark matter present in the galactic halos and should solely explain the observed rotational asymmetry seen towards the considered galaxies in the CMB by *Planck* data. Many models that explain the existence of this kind of small dense clouds have been proposed in the literature.

To take the matter of the true chemical composition and nature of virial clouds more physically, one would need to trace the cloud evolution from the time of their formation to the present, allowing for all the major qualitative changes that occurred during that time. Their formation would have been after the recombination time (that is at $z < 1000$), and they must have been in equilibrium

with the CMB since then. The first step of the evolution of these clouds from the surface of the last scattering (LSS) up to the formation of population-III stars has been studied in detail (Tahir et al. , 2021). In Ref. Bromm et al. (1999) hydrodynamic simulations were used to explain the formation of first-generation stars and investigate the fragmentation process of a metal-free gas. It was seen that this gas collapsed at $z = 30$ in clouds with a mass of about $10^6 M_{\odot}$. Fragmentation then led to the formation of dense clumps of mass about $10^3 M_{\odot}$. It was seen in Ref. (Tahir et al. , 2021) that at $z = 50$ virial clouds which are made of primordial gas have a mass of about $10^5 M_{\odot}$ which does not violate the results of Ref. Bromm et al. (1999). One could take the next step forward and move on towards evolution II of these clouds to understand their true nature, but the next step of evolution is more problematic and ambiguities can arise. At this stage, we will have to incorporate the quantum calculations that were found to be negligible in the Evolution I paper. All these things should be taken into account to understand if the virial cloud model used in this paper is not in contradiction with the models already present in literature for such kinds of clouds in the halos. This will be studied later in more detail.

Acknowledgments

We acknowledge the use of Planck’s data in the Legacy Archive for Microwave Background Data Analysis (LAMBDA) and HEALPix Gorski et al. (2005) packages. The TAsP and Euclid INFN projects are also acknowledged as well as the anonymous referees for the useful comments.

References

- Bertone, G. *Particle Dark Matter: Observations, Models and Searches*; Cambridge University Press: Cambridge, UK, 2010.
- Burduzha, V.V. From the Early Universe to the Modern Universe. *Symmetry* **2020**, *12*, 382.
- Pérez de los Heros, C. Status, Challenges and Directions in Indirect Dark Matter Searches. *Symmetry* **2020**, *12*, 1648.
- Shull, J.M.; Smith, B.D.; Danforth, C.W. The Baryon Census in a Multiphase Intergalactic Medium: 30% of the Baryons May Still be Missing. *Astrophys. J.* **2012**, *759*, 23.
- Driver, S. The challenge of measuring and mapping the missing baryons. *Nat. Astron.* **2021**, *5*, 852–854.
- Cen, R.; Ostriker, J.P. Where are the baryons? *Astrophys. J.* **1999**, *514*, 1–6.
- Cen, R.; Ostriker, J.P. Where are the baryons? II. Feedback effects. *Astrophys. J.* **2006**, *650*, 560–572.
- Fraser-McKelvie, A.; Pimbblet, K.A.; Lazendic, J.S. An estimate of the electron density in filaments of galaxies at $z \sim 0.1$. *Mon. Not. R. Astron. Soc.* **2011**, *415*, 1961–1966.
- Gupta, A., Mathur, S., Krongold, Y., Nicastro, F., Galeazzi, M. A Huge Reservoir of Ionized Gas around the Milky Way: Accounting for the Missing Mass? *Astrophys. J. Lett.* **2012**, *756*, L8.
- De Paolis, F.; Ingrassio, G.; Jetzer, P.; Roncadelli, M. A Case for a baryonic dark halo. *Phys. Rev. Lett.* **1995**, *74*, 14–17.
- Gerhard, O.; Silk, J. Baryonic Dark Halos: A Cold Gas Component? *Astrophys. J.* **1996**, *472*, 34.
- Pifenniger, D.; Combes, F.; Martinet, L. Is dark matter in spiral galaxies cold? *Astron. Astrophys.* **1994**, *285*, 79–93.
- Palla, F.; Salpeter, E.E.; Stahler, S.W. Primordial star formation: The role of molecular hydrogen. *Astrophys. J.* **1983**, *271*, 632–641.
- De Paolis, F.; Ingrassio, G.; Jetzer, P.; Roncadelli, M. A scenario for a baryonic dark halo. *Astron. Astrophys.* **1995**, *295*, 567.

- Dixon, D.D.; Hartmann, D.H.; Kolaczyk, E.D.; Samimi, J.; Diehl, R.; Kanbach, G.; Mayer-Hasselwander, H.; Strong, A.W., Evidence for a Galactic gamma-ray halo. *New Astron.* **1998**, *3*, 539–561.
- De Paolis, F.; Inghosso, G.; Jetzer, P.; Roncadelli, M. Gamma-Ray Astronomy and Baryonic Dark Matter. *Astrophys. J. Lett.* **1999**, *510*, L103–L106.
- Kalberla, P.M.W.; Shchekinov, Y.A.; Dettmar, R.J. H₂ dark matter in the galactic halo from EGRET. *Astron. Astrophys.* **1999**, *350*, L9–L12.
- Alcock, C.; Akerlof, C.W.; Allsman, R.; Axelrod, T. S.; Bennett, D. P.; Chan, S.; Cook, K.H.; Freeman, K.C.; Griest, K.; Marshall, S.L.; et al. Possible gravitational microlensing of a star in the Large Magellanic Cloud. *Nature* **1993**, *365*, 621–623.
- De Rújula, A.; Jetzer, P.; Massó, E. Dark mass moments. *Mon. Not. R. Astron. Soc.* **1991**, *250*, 348.
- De Paolis, F.; Inghosso, G.; Jetzer, P.; Qadir, A.; Roncadelli, M. Observing molecular hydrogen clouds and dark massive objects in galactic halos. *Astron. Astrophys.* **1995**, *299*, 647.
- De Paolis, F.; Gurzadyan, V.; Inghosso, G.; Jetzer, Ph.; Nucita, A. A.; Qadir, A.; Vetrugno, D.; Kashin, A.L.; Khachatryan, H.G.; Mirzoyan, S. Possible detection of the M 31 rotation in WMAP data. *Astron. Astrophys.* **2011**, *534*, L8.
- De Paolis, F.; Gurzadyan, V.; Nucita, A.A.; Inghosso, G.; Kashin, A. L.; Khachatryan, H.G.; Mirzoyan, S.; Poghosian, E.; Jetzer, Ph.; Qadir, A.; et al. Planck confirmation of the disk and halo rotation of M 31. *Astron. Astrophys.* **2014**, *565*, L3.
- De Paolis, F.; Gurzadyan, V.; Nucita, A.A.; Inghosso, G.; Kashin, A.L.; Khachatryan, H.G.; Mirzoyan, S.; Yegorian, G.; Jetzer, Ph.; Qadir, A.; et al. Planck revealed bulk motion of Centaurus A lobes. *Astron. Astrophys.* **2015**, *580*, L8.
- Gurzadyan, V.; De Paolis, F.; Nucita, A.A.; Inghosso, G.; Kashin, A.L.; Khachatryan, H.G.; Sargsyan, S.; Yegorian, G.; Jetzer, Ph.; Qadir, A.; et al. Planck view of the M 82 galaxy. *Astron. Astrophys.* **2015**, *582*, A77.
- De Paolis, F.; Gurzadyan, V.; Nucita, A.A.; Chemin, L.; Qadir, A.; Kashin, A.L.; Khachatryan, H.G.; Sargsyan, S.; Yegorian, G.; Inghosso, G.; et al. Triangulum galaxy viewed by Planck. *Astron. Astrophys.* **2016**, *593*, A57.
- Gurzadyan, V.; De Paolis, F.; Nucita, A.A.; Kashin, A.L.; Amekhyan, A.; Sargsyan, S.; Yegorian, G.; Qadir, A.; Inghosso, G.; Jetzer, Ph.; et al. Messier 81's Planck view versus its halo mapping. *Astron. Astrophys.* **2018**, *609*, A131.
- De Paolis, F.; Gurzadyan, A.; Nucita, A.A.; Gurzadyan, V. G.; Qadir, A.; Kashin, A.; Amekhyan, A.; Sargsyan, S.; Jetzer, Ph.; Inghosso, G.; et al. Rotating baryonic dark halos. *Astron. Astrophys.* **2019**, *629*, A87.
- Tahir, N.; De Paolis, F.; Qadir, A.; Nucita, A.A. Constraining Baryons in the M31 galactic halo by Planck data. *Int. J. Mod. Phys. D* **2019**, *28*, 1950088.
- Tahir, N.; De Paolis, F.; Qadir, A.; Nucita, A.A. Seeing the halo rotation of nearby spiral galaxies using Planck data. *Arab. J. Math.* **2019**, *8*, 193–199.
- Qadir, A.; Tahir, N.; Sakhi, M. Virial clouds explaining the observed rotational asymmetry in the galactic halos. *Phys. Rev. D* **2019**, *100*, 043028.
- ; Imara, N.; Loeb, A.; Johnson, B.D.; Conroy, C.; Behroozi, P. A Model Connecting Galaxy Masses, Star Formation Rates, and Dust Temperatures across Cosmic Time. *Astrophys. J.* **2018**, *854*, 36.
- Draine, B.T. Interstellar Dust Grains. *Annu. Rev. Astron. Astrophys.* **2003**, *41*, 241–289.
- Yershov, V.; Raikov, A.; Lovyagin, N.Y.; Kuin, N.P.M.; Popova, E.A. Distant foreground and the Planck-derived Hubble constant. *Mon. Not. R. Astron. Soc.* **2020**, *492*, 5052–5056.

- Ferrara, A.; Ferrini, F.; Franco, J.; Barsella, B. Evolution of Dust Grains through a Hot Gaseous Halo. *Astrophys. J.* **1991**, *381*, 137–146.
- Salpeter, E.E. Formation and flow of dust grains in cool stellar atmospheres. *Astrophys. J.* **1974**, *193*, 585–592.
- Kwok, S. Radiation pressure on grains as a mechanism for mass loss in red giants. *Astrophys. J.* **1975**, *198*, 583–591.
- Chiao, R.; Wickramasinghe, N. Radiation-driven efflux and circulation of dust in spiral galaxies. *Mon. Not. R. Astron. Soc.* **1972**, *159*, 361–373.
- Greenberg, J.M.; Ferrini, F.; Barsella, B.; Aiello, S. Is there dust in galactic haloes? *Nature* **1987**, *327*, 214–216.
- Barsella, B.; Ferrini, F.; Greenberg, J.; Aiello, S. Large-scale behavior of dust grains in a galactic environment. *Astron. Astrophys.* **1989**, *209*, 349–360.
- Hirashita, H.; Lin, C.Y. Dust abundance and grain size in galaxy halos. *Planet. Space Sci.* **2020**, *183*, 104504.
- Navarro, J.F.; Frenk, C.S.; White, S.D.M. The Structure of Cold Dark Matter Halos. *Astrophys. J.* **1996**, *462*, 563.
- Moore, B.; Ghigna, S.; Governato, F.; Lake, G.; Quinn, T.; Stadel, J.; Tozzi, P. Dark Matter Substructure within Galactic Halos. *Astrophys. J. Lett.* **1999**, *524*, L19–L22.
- Burkert, A. The Structure of Dark Matter Halos in Dwarf Galaxies. *Astrophys. J. Lett.* **1995**, *447*, L25–L28.
- Tamm, A.; Tempel, E.; Tenjes, P.; Tihhonova, O.; Tuvikene, T. Stellar mass map and dark matter distribution in M 31. *Astron. Astrophys.* **2012**, *546*, A4.
- Lokas, E.L.; Mamon, G.A. Properties of spherical galaxies and clusters with an NFW density profile. *Mon. Not. R. Astron. Soc.* **2001**, *321*, 155–166.
- Lehner, N.; Berek, S.C.; Howk, J.C.; Wakker, B.P.; Tumlinson, J.; Jenkins, E.B.; Prochaska, J.X.; Augustin, R.; Ji, S.; Faucher G.; et al. Project AMIGA: The Circumgalactic Medium of Andromeda. *Astrophys. J.* **2020**, *900*, 9.
- Carignan, C.; Chemin, L.; Huchtmeier, W.K.; Lockman, F.J. The extended HI rotation curve and mass distribution of M31. *Astrophys. J. Lett.* **2006**, *641*, L109–L112.
- Gorski, K.M.; Hivon, E.; Banday, A.J.; Wandelt, B. D.; Hansen, F. K.; Reinecke, M.; Bartelmann, M. HEALPix: A Framework for High-Resolution Discretization and Fast Analysis of Data Distributed on the Sphere. *Astrophys. J.* **2005**, *622*, 759–771.
- Matilla, J.M.Z.; Haiman, Z.; Probing gaseous galactic halos through the rotational kinematic Sunyaev-Zeldovich effect. *Phys. Rev. D* **2020**, *101*, 083016.
- Dolag, K.; Enlin, T.A. Radio halos of galaxy clusters from hadronic secondary electron injection in realistic magnetic field configurations. *Astron. Astrophys.* **2000**, *362*, 151–157.
- Sun, X.H.; Reich, W. The Galactic halo magnetic field revisited. *Res. Astron. Astrophys.* **2010**, *10*, 1287–1297.
- Leitch, E.M.; Readhead, A.C.R. The Discovery of Anomalous Microwave Emission. *Adv. Astron.* **2013**, *2013*, 352407.
- Tahir, N.; Qadir, A.; De Paolis, F.; Nucita, A.A. The rotational kinetic Sunyaev-Zeldovich contribution to the temperature asymmetry toward the M 31 halo. *Astron. Astrophys.* **2022**, *664*, A30.
- Tahir, N.; Qadir, A.; Sakhi, M.; De Paolis, F. Evolution of virial clouds-I: from surface of last scattering up to the formation of population-III stars. *Eur. Phys. J. C* **2021**, *81*, 827.
- Bromm, V.; Coppi, P.S.; Larson, R.B. Forming the first stars in the Universe: The fragmentation of primordial gas. *Astrophys. J.* **1999**, *527*, L5–L8.